Frequency-specific network activity predicts bradykinesia severity in Parkinson's disease

Muthuraman Muthuraman, Marcell Palotai, Borbála Jávor-Duray, Andrea Kelemen, Nabin Koirala, László Halász, Loránd Erőss, Gábor Fekete, László Bognár, Günther Deuschl, Gertrúd Tamás

Angaben zur Veröffentlichung / Publication details:

Muthuraman, Muthuraman, Marcell Palotai, Borbála Jávor-Duray, Andrea Kelemen, Nabin Koirala, László Halász, Loránd Erőss, et al. 2021. "Frequency-specific network activity predicts bradykinesia severity in Parkinson's disease." *NeuroImage: Clinical* 32 (5): 102857. https://doi.org/10.1016/j.nicl.2021.102857.

NeuroImage: Clinical 32 (2021) 102857

Contents lists available at ScienceDirect

NeuroImage: Clinical

journal homepage: www.elsevier.com/locate/ynicl

Frequency-specific network activity predicts bradykinesia severity in Parkinson's disease

Muthuraman Muthuraman [a], Marcell Palotai [b], Borbála Jávor-Duray [b], Andrea Kelemen [b], Nabin Koirala [a,c], László Halász [d], Loránd Erőss [d], Gábor Fekete [e], László Bognár [e], Günther Deuschl [f], Gertrúd Tamás [b,*]

[a] Movement Disorders, Imaging and Neurostimulation, Biomedical Statistics and Multimodal Signal Processing, Department of Neurology, University Medical Center of the Johannes Gutenberg University, Mainz, Germany
[b] Department of Neurology, Semmelweis University, Budapest, Hungary
[c] Haskins Laboratories, New Haven, USA
[d] National Institute of Clinical Neurosciences, Budapest, Hungary
[e] Department of Neurosurgery, University of Debrecen, Debrecen, Hungary
[f] Department of Neurology, Christian-Albrechts University, Kiel, Germany

ARTICLE INFO

Keywords:
Beta oscillation
Gamma oscillation
Bradykinesia
Parkinson disease
Deep brain stimulation

ABSTRACT

Objective: Bradykinesia has been associated with beta and gamma band interactions in the basal ganglia-thalamocortical circuit in Parkinson's disease. In this present cross-sectional study, we aimed to search for neural networks with electroencephalography whose frequency-specific actions may predict bradykinesia.
Methods: Twenty Parkinsonian patients treated with bilateral subthalamic stimulation were first prescreened while we selected four levels of contralateral stimulation (0: OFF, 1–3: decreasing symptoms to ON state) individually, based on kinematics. In the screening period, we performed 64-channel electroencephalography measurements simultaneously with electromyography and motion detection during a resting state, finger tapping, hand grasping tasks, and pronation-supination of the arm, with the four levels of contralateral stimulation. We analyzed spectral power at the low (13–20 Hz) and high (21–30 Hz) beta frequency bands and low (31–60 Hz) and high (61–100 Hz) gamma frequency bands using the dynamic imaging of coherent sources. Structural equation modelling estimated causal relationships between the slope of changes in network beta and gamma activities and the slope of changes in bradykinesia measures.
Results: Activity in different subnetworks, including predominantly the primary motor and premotor cortex, the subthalamic nucleus predicted the slopes in amplitude and speed while switching between stimulation levels. These subnetwork dynamics on their preferred frequencies predicted distinct types and parameters of the movement only on the contralateral side.
Discussion: Concurrent subnetworks affected in bradykinesia and their activity changes in the different frequency bands are specific to the type and parameters of the movement; and the primary motor and premotor cortex are common nodes.

1. Introduction

The pathophysiological mechanisms in the brain in relation to bradykinesia are extensively examined in Parkinson's disease (de Hemptinne et al., 2015; Neumann et al., 2016) and its animal models (Mallet et al., 2008; West et al., 2018). Alterations in oscillatory activities within the basal ganglia-thalamocortical loop, (Kühn et al., 2008; Hirschmann et al., 2013; Lalo et al., 2008; Pollok et al., 2013) suggested modified system dynamics in Parkinson's disease, which could be influenced by dopaminergic (Hirschmann et al., 2013; Lalo et al., 2008) and deep brain stimulation (Kühn et al., 2008) therapy.

Excessive beta band (13–30 Hz) activity seems to have an imperator

Abbreviations: M1, primary motor cortex; PMC, premotor cortex; DLPFC, dorsolateral prefrontal cortex; SMA, supplementary motor cortex; STN, subthalamic nucleus; CER, cerebellum; PPC, posterior parietal cortex; FT, finger tapping; PS, pronation-supination; HG, hand grasping; StrEM, structural equation modelling.

* Corresponding author at: Department of Neurology, Semmelweis University, Balassa utca 6., Budapest 1083, Hungary.
E-mail address: tamas.gertrud@med.semmelweis-univ.hu (G. Tamás).

https://doi.org/10.1016/j.nicl.2021.102857
Received 28 March 2021; Received in revised form 15 September 2021; Accepted 12 October 2021
Available online 13 October 2021

role in the compound network oscillations in Parkinson's disease (Neumann et al., 2016; Wang et al., 2018). Human local field potential measurements pointed out that high beta activity in the subthalamic nucleus positively correlates with the motor impairment on the group level, across patients (Neumann et al., 2016), as well as in a repeated measures design within patients (Steiner et al., 2017; Williams et al., 2005). Similarly, a decrease of beta power after levodopa therapy (Kühn et al., 2009; Ray et al., 2008) and deep brain stimulation (DBS) sessions (Kühn et al., 2008; Oswal et al., 2016) correlated with the improvement of contralateral bradykinesia and rigidity. Prominent beta activity in the motor cortex was also related to dopamine depletion in animal models and in humans (Mallet et al., 2008; Whitmer et al., 2012). However, a correlation analysis between the changes in frontal cortical beta power and the changes of movement parameters on a group level has resulted in controversial conclusions (Oswal et al., 2016; Abbasi et al., 2018; Luoma et al., 2018; Pollok et al., 2012).

Unlike beta activity, gamma synchronization may promote the information processing in functionally connected neuronal circuits (Tamás et al., 2018). A narrow band gamma (60–90 Hz) activity was found to be coherent between the STN and the primary motor cortex in Parkinson's disease during movement (Litvak et al., 2012). In this band, the change in subthalamic nucleus (STN) power (Litvak et al., 2012; Lofredi et al., 2018) and the STN-primary motor cortex (M1) coherence (Litvak et al., 2012) after levodopa treatment correlated with the bradykinesia and rigidity (Litvak et al., 2012). The narrow band gamma activity measured in the M1 and the STN was also linked to hyperkinesia in Parkinson's disease (Swann et al., 2016). Movement-induced broadband gamma (30–100 Hz) activity was detected in the STN and the M1 contralateral to the movement in Parkinson's disease (Litvak et al., 2012); the amplitude of the cortical gamma oscillation is coupled to the STN beta phase (Shimamoto et al., 2013). The STN gamma activity did not correspond to the clinical symptoms (Lofredi et al., 2018).

Studies analysing STN local field potential and electrocorticography focused on the primary sensorimotor area (de Hemptinne et al., 2015; Whitmer et al., 2012); this cortical location for OFF state-related neurophysiological markers was also confirmed by magnetoencephalography and EEG studies beside the premotor cortex or the supplementary motor cortex (SMA) (Oswal et al., 2016; Abbasi et al., 2018; Luoma et al., 2018; Litvak et al., 2012). The entire network, including the cortico-subcortical regions, has not been analyzed simultaneously in any of the above studies.

In this current study we aimed to explore motor cortical areas and their networks with EEG, in which beta or gamma band activity may predict bradykinesia in Parkinsonian patients to further explore its pathophysiology. The novelty of the current study is that we investigated Parkinsonian patients treated with bilateral STN-DBS that allowed the testing of different levels of bradykinesia resulted by different levels of stimulation on the individual level. The recruited patients were chronically stimulated, so the stun effect of the early postoperative phase, which was shown to cause temporary and frequency-specific alterations in STN activity (Rosa et al., 2010), did not influence our results. We captured different parameters of bradykinesia (i.e., speed, amplitude, rhythm, and decrement in speed and amplitude) objectively with motion analysis as their abnormalities may reflect different pathophysiological processes (Bologna et al., 2020). We related their changes to the evolution of network activities individually.

We hypothesized that different subnetwork activities are involved in developing distinct bradykinesia components on their own preferred frequencies (Tamás et al., 2018).

2. Methods

2.1. Participants

Twenty Parkinsonian patients treated with bilateral STN-DBS were recruited for the study, with a minimum of 1 year of follow-up after the operation. They had Kinetra and Activa PC stimulator implants with leads No. 3389 (Medtronic plc.). Dementia and musculoskeletal diseases leading to disabilities were exclusion criteria. The patients signed an informed consent form according to the Declaration of Helsinki. The Medical Research Council in Hungary has provided ethical approval (080958/2015/OTIG). The study protocol is summarized in Fig. 1.

2.2. Prescreening

A prescreening was performed the day before the screening for all patients with motion analysis. The contralateral STN was first in the stimulation OFF condition, and then ON conditions, in which the clinically most effective contact was activated from 0,5V to the voltage limit with side effects up to 4 V with 0,5V steps. We calculated Kinesia scores separately for the speed, amplitude, and rhythm of the movements (Espay et al., 2011; Heldman et al., 2011); these values were then averaged across the three parameters and tasks, creating a total Kinesia score (Pulliam et al., 2015) for each patient for each stimulation step. We sorted out four different Kinesia total score values and their associated stimulation intensities individually and assigned a level of contralateral stimulation (0: OFF, 1–3: gradual improvement of bradykinesia to the optimal ON state) to these values (Fig. 2, Table 1).

2.3. Screening

On the second day, in the screening period, we conducted 64-channel EEG measurements simultaneously with EMG and motion detection of the movements of the more affected hand. One bipolar surface EMG channel measured the activity of the forearm extensors and one of the biceps brachii muscle. We screened the patients during RESTING STATE (sitting in a supine position with eyes open and fixed to a point ahead) and then FINGER TAPPING, PRONATION-SUPINATION, and HAND GRASPING of the more affected upper limb. Patients repeated the task series on the four levels of contralateral stimulation, which were selected in the prescreening period, in counterbalanced order.

2.4. Surgical procedure

The STN target was selected using standard stereotactic procedures (Andrade-Souza et al., 2005) according to individual anatomical structures; electrode implantation was guided by microelectrode recording and clinical testing during macrostimulation in each patient (detailed description in (Tamás et al., 2016)).

2.5. Estimation of the volume of tissue activated (VTA)

All patients underwent pre-operative MRI, using a 3 Tesla MRI scanner (Philips Achieva) with an 8-channel SENSE head coil under general anesthesia avoiding movement artifacts. The pre-operative MRI included the whole-brain high resolution T1-images using standard MPRAGE (magnetization-prepared 180 degrees radio-frequency pulses and rapid gradient-echo) sequence with TR = 9.6031 ms, TE = 4.6 ms, flip angle = 80 and voxel resolution of 1 × 1 × 1 mm3. The post-operative CT scan was performed using Siemens SOMATOM-Definition-AS-plus scanner with axial slices of slice thickness of 1 mm one month after operation.

To verify the optimal location of the stimulation, we localized the active contact and estimated the volume of tissue activated (VTA) individually in the different stimulation levels. We estimated VTA using lead DBS - a Matlab based toolbox for reconstructing the implanted electrodes and simulating the stimulation (https://www.lead-dbs.org/). The details of electrode localization and VTA reconstruction have previously been described (Horn and Kühn, 2015; Horn et al., 2019). In brief, preprocessing was performed using SPM12 (http://www.fil.ion.ucl.ac.uk/spm/software/spm12) where postoperative images were linearly co-registered to preoperative MRI and were manually controlled

Prescreening

- **Measuring Device: 3D gyroscope**
- Medication withdrawal
- More affected hand is examined
- The clinically most effective contact is stimulated
- Ipsilateral stimulation remains stable
- Contralateral stimulation is set from 0 to 3.5V with 0,5V steps

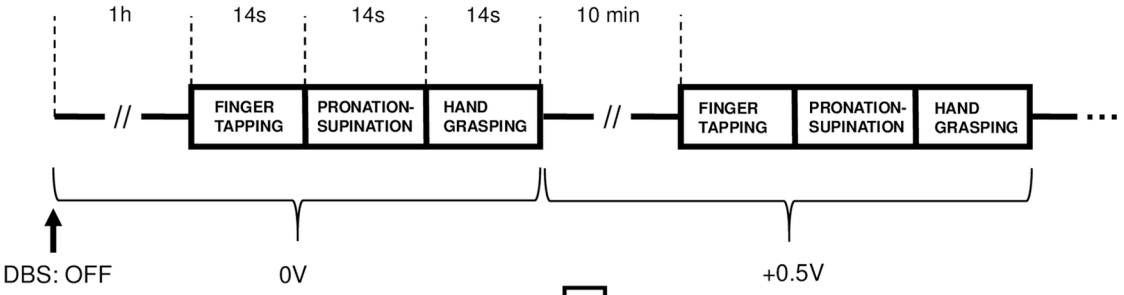

Four levels of contralateral stimulation were selected:
0: STIM OFF
1: slight improvement of bradykinesia
2: moderate improvement
3: maximum improvement

Screening

- **Measuring Device: 64 channel EEG and 3D gyroscope + 2-ch EMG**
- Medication withdrawal
- More affected hand is examined
- The clinically most effective contact is stimulated
- Ipsilateral stimulation remains stable
- Contralateral stimulation is set to the selected 0, 1, 2, 3 levels in randomized order

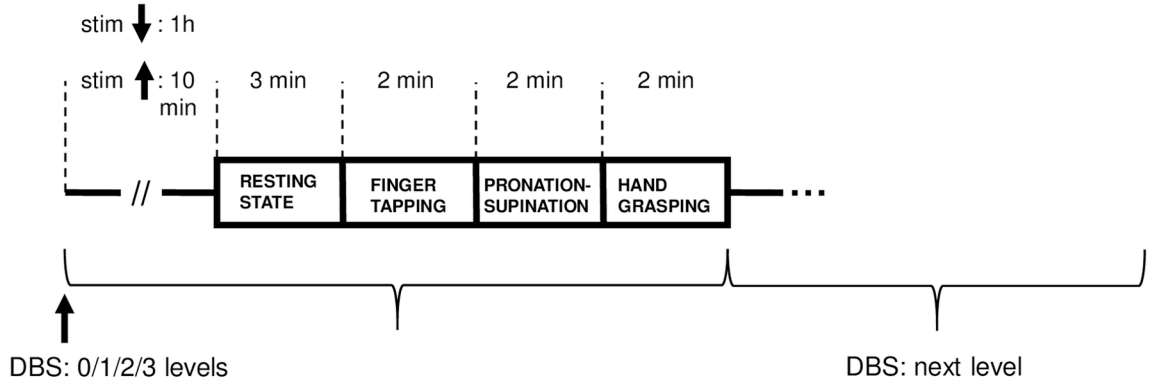

Fig. 1. Study protocol.

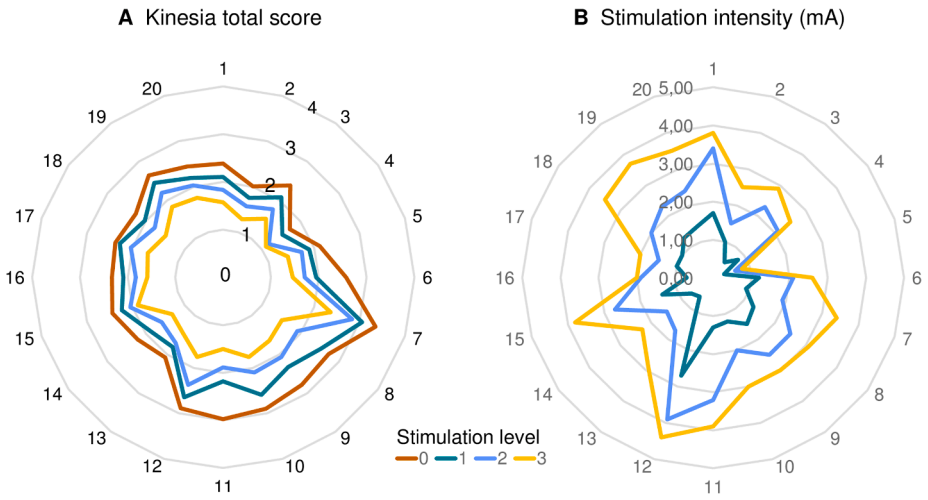

Fig. 2. Selecting stimulation levels on the prescreening day A. Kinesia total scores on the four stimulation levels assigned on the prescreening day (stimulation off state: level 0, stimulation on states: levels 1–3) in the 20 patients. B. Stimulation intensity on the four levels of stimulation in the 20 patients. Kinesia total scores (A) and stimulation intensities (B) are presented on the radial axis while the number of patients on the outer angular axis.

Table 1
Statistical analysis comparing the Kinesia combined scores across the three tasks and four stimulation levels.

Within factor			Post hoc comparisons; CI 95% of the mean differences
TASK	$F_{2,38}$ = 1.74	p = 0.19	
STIMULATION LEVEL	$F_{3,57}$ = 194.33	p < 0.001	All comparisons: p < 0.001; 0–1: 0.25–0.35 0–2: 0.5–0.64 0–3: 0.8–0.97 1–2: 0.23–0.31 1–3: 0.52–0.65 2–3: 0.26–0.36

for each patient and refined when needed. Thus, obtained images were then normalized into ICBM 2009b NLIN asymmetric space based on the preoperative MRI; finally, DBS electrode contacts were localized within the MNI space using Lead-DBS software. To construct a model for volume conduction of the DBS electrode from the active contact, a tetrahedral volume mesh was generated based on the surface meshes of DBS electrodes and subcortical nuclei using the Iso2Mesh toolbox (http://iso2mesh.sourceforge.net/), as included in Lead-DBS. All of the parameters used for the reconstruction have previously been published (Horn et al., 2017); the voltage applied to the active electrode contacts was introduced as a boundary condition (Åström et al., 2009).

2.6. Kinematic analysis

A Kinesia (Great Lakes NeuroTechnologies Inc., Cleveland, OH) motion sensor system consisting of a three-dimensional gyroscope was fixed on the index finger of the subject to capture kinematic parameters of movements in each stimulation steps (Espay et al., 2011; Heldman et al., 2011). Analysis of the motion data is described in Ref (Tamás et al., 2016). Speed as the root mean square angular velocity, amplitude as the root mean square excursion angle, and the rhythm as the coefficient of variation were calculated (Espay et al., 2011; Heldman et al., 2011; Tamás et al., 2016). A higher coefficient of variation is a sign of worse rhythmicity. The values of speed, amplitude, and rhythm were converted to Kinesia scores (0–4 on continuous scale; a higher score represents more severe bradykinesia) (Espay et al., 2011), which were then used for further analysis. We also computed the decrement of speed and amplitude from the relevant Kinesia scores as traits of bradykinesia in Parkinson's disease; they were the ratios of the values in the fourth 30 sec. time interval to the values in the first 30 sec. for each 2 min. task.

2.7. EEG acquisition, preprocessing and time frequency analyses

EMG was recorded in parallel with a standard 64-channel EEG recording system (Brain Products Co., Munich, Germany) using a linked vertex reference. A standard EEG cap was used with electrodes positioned according to the extended 10–20 system. The pre-processing steps were performed by a researcher who was blinded to the stimulation conditions. EEG data preprocessing and part of the spatial filter analysis were performed using MATLAB2018a and the fieldtrip toolbox (Oostenveld et al., 2011). Initially, EEG data was re-referenced to the common grand average reference of all EEG channels. The raw EEG data was low-pass filtered (fourth-order Butterworth filter; cut-off frequency: 300 Hz) to avoid aliasing, followed by high pass filtering at 0.5 Hz. A notch filter was used to filter out the 50, 100, and 150 Hz activity. In the second step, EEG data was subjected to independent component analysis (FastICA) to remove the components representing the DBS artifacts, muscle artifacts, eye blinks, eye movements, and line noise. On average, for the experiments, 8 of 64 components (8 ± 2.3, mean ± SD) were rejected, 2–3 were related to DBS artifacts (2 ± 1.24), 1–2 were related to eye artifacts (1 ± 0.68), 1–2 related to line noise (1 ± 0.34) and 1–2 were related to muscle artifacts (1 ± 1.21). The residual muscle artifacts were visually inspected, removed, and interpolated with the cubic interpolation method. Continuous data was first decomposed into time–frequency representation by using the multitaper method (Mitra and Pesaran, 1999; Muthuraman et al., 2010). In this method the spectrum is estimated by multiplying the data with different windows (i.e. tapers). In this study orthogonal tapers were used with optimal leakage and spectral properties, along with the applied discrete prolate spheroidal sequences (Slepian and Pollak, 1961). EMG was band-pass filtered (30–200 Hz), a notch filter was used; it was sampled at 1000 Hz. The data was stored in a computer and analysed off-line. The EMG was full-wave rectified (Muthuraman et al., 2010).

2.8. EEG source analyses

The reconstruction of the brain activity used the forward solution with a finite-element method (Wolters et al., 2007). A full description of the beamformer linear constrained minimum variance spatial filter is given elsewhere (Muthuraman et al., 2018; Van Veen et al., 1997).

The forward problem is the computation of the scalp potentials for a

set of neural current sources. An established procedure was used by estimating the lead-field matrix with specified models for the brain; a volume conduction model with a finite-element method was used (Wolters et al., 2007). For the forward modelling the surfaces of the compartments, such as the skin, skull, cerebrospinal fluid, and the white matter were extracted from the individual T1 MRI scans, and individual electrode locations were used. The forward modelling and the source analysis were done in FieldTrip (Oostenveld et al., 2011). The lead-field matrix contains information about the geometry and conductivity of the model. The complete description of the solution for the forward problem has been described previously (Muthuraman et al., 2010; Muthuraman et al., 2012). A full description of the beamformer linear constrained minimum variance spatial filter is given elsewhere (Muthuraman et al., 2018; Van Veen et al., 1997). The output of the beamformer at a voxel in the brain can be defined as a weighted sum of the output of all EEG channels. The weights determine the spatial filtering characteristics of the beamformer and are selected to increase the sensitivity to signals from a voxel and reduce the contributions of signals from (noise) sources at different locations. The frequency components and their linear interactions are represented as a cross-spectral density matrix. In order to visualize power at a given frequency range, a linear transformation was used based on a constrained optimization problem that acts as a spatial filter (Van Veen et al., 1997). The spatial filter assigned a specific value of power to each voxel. For a given source the beamformer weights for a location of interest are determined by the data covariance matrix and the lead-field matrix. A voxel size of 5 mm was used in this study, resulting in 3676 voxels covering the entire brain. We estimated the coherent sources involved in the FINGER TAPPING task, namely four cortical (M1, PMC, SMA, DPFC) and two sub-cortical regions (STN and cerebellum: CER) for each patient separately based on the EMG signal as reference. The individual MNI co-ordinates of these regions were then used for analysis of the RESTING STATE and other movement tasks. We used the FINGER TAPPING task as our reference task because previous publications from our group and other centers revealed robust networks of this task in healthy controls (Anwar et al., 2016; Muthuraman et al., 2014; Pollok et al., 2007; Pollok et al., 2009). For each frequency band, the activated voxels were selected by a within-subject surrogate analysis to define the significance level, which was then used to identify voxels in the regions as activated voxels. Once the brain region voxels were identified, their activities were extracted from the source space. In a further analysis, all the original source signals for each region with several activated voxels were combined by estimating the second order spectra and employing a weighting scheme depending on the analysed frequency range to form a pooled source signal estimate for each region as previously described (Muthuraman et al., 2014; Amjad et al., 1997; Rosenberg et al., 1989; Muthuraman et al., 2020).

We computed the absolute power at four different frequency bands, namely low beta (13–20 Hz), high beta (21–30 Hz) (Lofredi et al., 2019), low gamma (31–60 Hz) and high gamma (61–100 Hz) (Cao et al., 2017) bands at each of the six regions separately. We calculated the absolute power values both contralateral and ipsilateral to the movement during RESTING STATE, FINGER TAPPING, HAND GRASPING and PRONATION-SUPINATION tasks.

2.9. Statistical analysis

Normal distribution of the data sets was tested by the Kolmogorov-Smirnov test. For demographic data and therapeutic information, we used descriptive statistics (mean, median and standard error of mean).

In the screening period, we compared the speed, amplitude, and the decrement of the speed and amplitude, and the rhythm separately at the four stimulation levels in each task. We analysed the power of the beta and gamma bands in the three tasks with ANOVA for repeated measures and the Newman-Keuls post hoc test. The within group effects were as follows: STIMULATION LEVEL and TASK for the kinematic data; LOCATION in the brain, BAND (beta and gamma), SUBBAND (low and high frequency range), STIMULATION LEVEL (0–3), TASK and HEMISPHERE (contralateral and ipsilateral to the examined more affected hand) for the EEG power values.

2.10. Structural equation modelling (StrEM) and statistics

The structural equation modelling (StrEM) analysis was performed in a toolbox for MATLAB (version 13a, Mathworks, Natick, MA, USA). StrEM represents a complex analytical tool that enables a determination between the causal relationships of the variables in a model-based approach. The relationship between the four analysed frequency bands and the Kinesia scores (speed, amplitude and rhythm) were assessed separately for each task in four different models. We estimated the slope of the trend lines of the Kinesia scores for movement speed, amplitude, and rhythm through the stimulation conditions (from 0 to 3); we used the following equation: Slope $= (y2 - y1)/(x2 - x1)$. Similarly, we calculated the slope of the trend lines of power in each frequency band. We used the slope of the power as input and slope of the Kinesia scores as output in the StrEM models.

We employed the Maximum Likelihood method of estimation to fit the models. To adjust the models for a large sample size, we used the Root Mean Square Error of Approximation index, which improves precision without increasing bias. The index estimates lack of fit in a model compared to a perfect model and therefore should be low. The index for all models was below 0.05, which indicates a very good fit for the models. In all models, the Invariant under a Constant Scaling and its factor criteria should be close to zero, which will signify that models were appropriate for analysis. Finally, using the Akaike Information Criterion, the quality of each model relative to other models was estimated, with smaller values signifying a better fit for the model. The obtained criterion comparing the models varied between 0.02 and 0.04 (which indicates a good fit for the models). The strength of associations between the variables in the models was quantified by standardized coefficients (s), ranging from 0 (no association) to 1 (very strong association). In addition to the AIC for the multiple models, we have controlled the results; the adjusted Bonferroni correction severity of the adjustment was weakened with an increasing value of the average absolute correlation between two parameters in the model (Smith and Cribbie, 2013). The described significant models survived the adjusted Bonferroni correction with ($p < 0.005$).

Table 2
Demographics and clinical data of the recruited patients.

Age mean (SD)		63.9 (8.62) years
Gender		5 females, 15 males
Disease duration		14.7 (7.56) years
Elapsed time after operation		3.05 (2.28) years
Left STN stimulation	Amplitude	2.3 (0.62) V
	Pulse width	60 (7.8) μs
	Frequency	132.5 (5.38) Hz
Right STN stimulation	Amplitude	2.3 (0.57) V
	Pulse width	61.4 (10.3) μs
	Frequency	132.5 (5.38) Hz
Tested STN		9 right, 11 left
Preoperative UPDRS III.	MED OFF	35.6 (18.59) points
	MED ON	7.9 (8.06) points
UPDRS III. at the time of the study	STIM ON-MED OFF	8.2 (7.26) points
	STIM ON-MED ON	4.2 (3.85) points
Hoehn-Yahr stage	Preoperative	2.6 (0.85)
	At the study	1.2 (0.63)
Levodopa equivalent dose	Preoperative	1017.5 (454.27) mg
	At the study	385.3 (172.99) mg

STN: subthalamic nucleus, UPDRS: Unified Parkinson's Disease Rating Scale.

3. Results

3.1. Clinical characteristics of the patients

Clinical characteristics of the patients are summarized in Table 2.

The active contacts located within the sensorimotor region of the STN in all subjects (Fig. 3).

3.1.1. Screening period, kinematic analysis:

The Kinesia scores of the speed did not differ in the different tasks. The speed and amplitude Kinesia scores decreased with rising stimulation intensity (Fig. 4). The Kinesia score of the rhythm improved the least among kinematic parameters by increasing stimulation intensity. The decrement of speed and amplitude did not differ in tasks and did not change with adjustment of stimulation intensity (Fig. 5).

3.1.2. Screening period, beta, and gamma power analysis:

The grand average power topographies of all the 20 patients are shown in Supplementary Fig. 1 for the finger tapping task, including a control region (posterior parietal cortex). In addition, we present the power spectrum for each region separately in all the four frequency bands and different tasks in Supplementary Fig. 2(A–G).

The elevation of stimulation intensity caused a significant decrease of beta power and increase of gamma power sequentially contralateral to the movement in the cortical areas and the STN, and ipsilateral in the cerebellum (Table 3, Figs. 6 and 7, Supplementary Fig. 3).

Beta power was higher than gamma power in the measurements. Beta and gamma power were lower in the continuously stimulated hemisphere ipsilateral to the examined hand than in the contralateral hemisphere during the whole measurement.

Low beta power was the highest in the M1, DLPFC and the CER, and was significantly different from low beta power in the PMC, SMA and STN. The high beta power in the M1, PMC, the DLPFC and the CER was significantly higher than in the SMA and the STN. The low and high band gamma power was similar in the M1, the PMC, the DLPFC, and the CER in the tasks and stimulation conditions; they were significantly higher than in the SMA and the STN. The high frequency beta/gamma power was significantly higher than low frequency beta/gamma power in their respective locations. Beta power was highest in the FINGER TAPPING and PRONATION-SUPINATION tasks, while gamma power in the FINGER TAPPING task in comparisons with the RESTING STATE and other movement tasks according to the overall ANOVA results including all locations and subbands. Power of beta and gamma activity was highest in the M1, DLPFC and the cerebellum, which was complemented by the SMA in FINGER TAPPING, and the PMC in PRONATION-SUPINATION task. Low and high-frequency beta and gamma activity did not change during movement compared to the resting state in the six locations and four stimulation conditions (all post hoc comparisons: $p > 0.05$; Figs. 6 and 7, Supplementary Fig. 3).

3.1.3. Structural equation modelling results

The obtained fit indices in the Structural equation modelling analysis implied a good fit for the constructed models to the observed data, providing robust causal relations between the variables.

In the FINGER TAPPING task, the input slope of low beta absolute power values from the network of M1 and PMC with STN as mediator were strong predictors for the slope of speed (standardized coefficient $S = 0.68$; $p < 0.005$) and the slope of amplitude ($S = 0.65$; $p < 0.005$), as shown in Fig. 8A in the first Structural equation model. In the second model for high gamma activity the input slope of high gamma power values from the network of PMC and DLPFC with CER as a mediator strongly linked to the slope of amplitude ($S = 0.62$; $p < 0.005$; Fig. 8B). In both models, the values from single cortical sources were not associated with the values of the STN (M1: $S = 0.26$; $p = 0.42$; PMC: $S = 0.31$; $p = 0.29$) or the CER (PMC: $S = 0.27$; $p = 0.39$; DLPFC: $S = 0.32$; $p = 0.31$).

In the third model for PRONATION-SUPINATION task, the slope of the high beta power values from the network of M1 and PMC with STN as mediator were strong predictors for the slope of amplitude ($S = 0.74$; $p < 0.005$); it is presented in Fig. 8C.

In the fourth model for HAND GRASPING task the slopes of the low beta power values from the circle consisting of M1 and SMA with STN as mediator were strong predictors for the slope of amplitude ($S = 0.81$; $p < 0.005$; Fig. 8D). In both models, the single sources were not associated

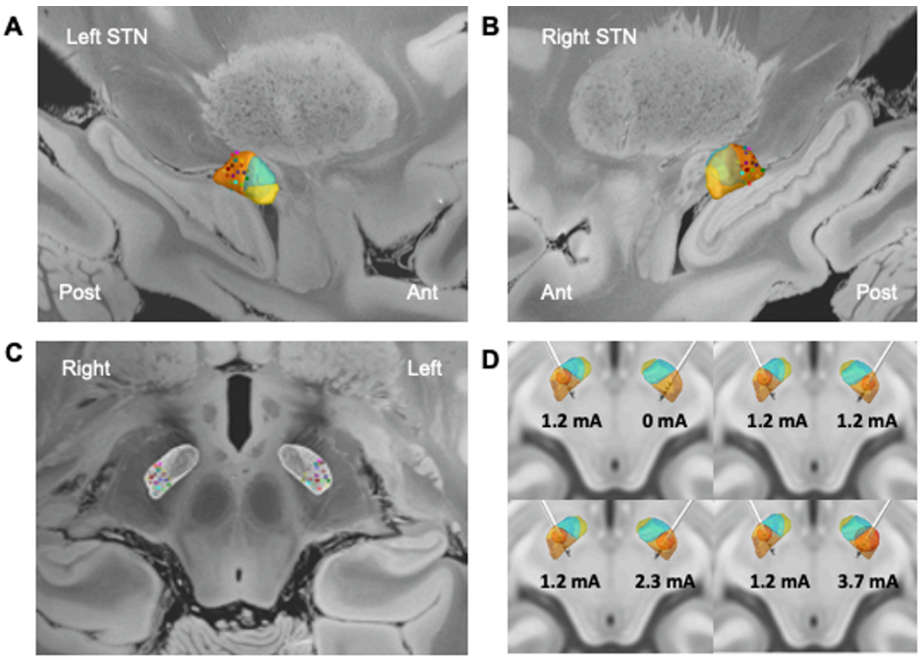

Fig. 3. Active contact locations and the volume of tissue activated in a representative patient Active contacts were in the sensorimotor part of the subthalamic nucleus in all patients (A–C). Background template: a 7 T MRI ex vivo 100-μm human brain. D. The volume of tissue activated in a representative patient, using 3 T anatomical T1 image. Orange: sensorimotor, blue: associative, yellow: limbic part of the STN.

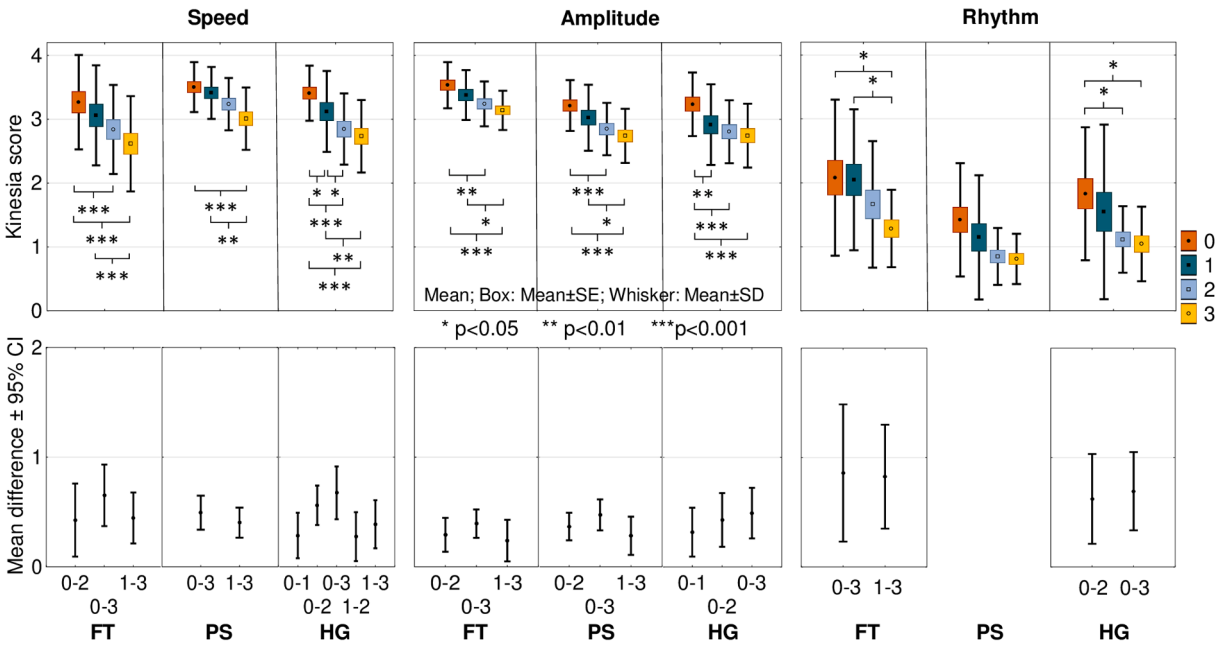

Fig. 4. Kinesia scores for speed, amplitude, and rhythms during screening The Kinesia scores are presented in the three movement tasks on the four stimulation levels (0–3). Speed and amplitude Kinesia scores decreased with increasing stimulation, the rhythm was the least affected.

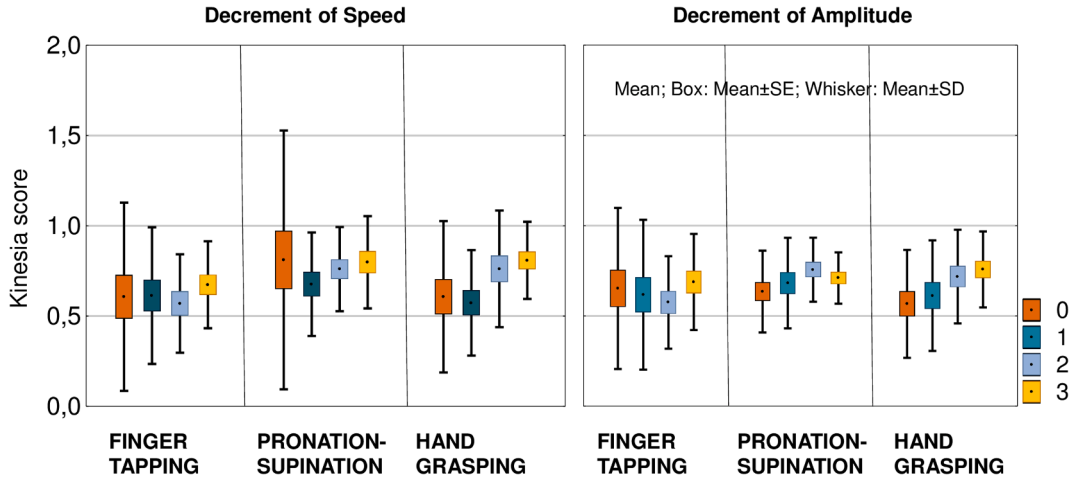

Fig. 5. Decrement of speed and amplitude Kinesia scores during screening Decrement of speed and amplitude as features of bradykinesia in the three tasks on the four stimulation levels (0–3). These parameters were not affected by the stimulation intensity and were similar in the different tasks.

with STN (third model: M1: S = 0.30; p = 0.52; PMC: S = 0.28; p = 0.18; fourth model: M1: S = 0.24; p = 0.34; SMA: S = 0.31; p = 0.28).

We have listed all ranges of the standardized coefficients from the SEM models obtained for each possible combination separately for each frequency band and task in Supplementary Tables 1–12.

4. Discussion

Our EEG study involving Parkinsonian patients with bilateral STN-DBS implants revealed that bradykinesia of the upper limb can be predicted the best from the beta and gamma activities of different sub-networks consisting predominantly of the primary motor, premotor cortex, and the STN. Increasing STN stimulation decreases beta power, and increases gamma power in the whole cortico-subcortical network parallel with the improvement of bradykinesia. According to the results, STN-DBS exerts strict ipsilateral effect on motor cortex areas during bilateral stimulation.

In line with other studies, our results confirm that several loops operate parallel in the motor system (Tamás et al., 2016) on their specific frequencies (Oswal et al., 2016; Litvak et al., 2011).

4.1. Network activity behind bradykinesia

Our results yielded the significance of the M1-PMC-STN network in the generation of beta activity in predicting bradykinesia in Parkinson's disease. We also detected a network, including the SMA, M1, and STN, whose low beta activity changes predicted the slope of hand grasping amplitude.

The beta activity in Parkinson's disease has already been supposed to originate in networks (Mallet et al., 2008; West et al., 2018), possibly along the hyperdirect pathway (West et al., 2018). It is supported by different findings. Coherent activity in the beta band has already been identified between M1, PMC and the STN (Oswal et al., 2016; Whitmer et al., 2012; Litvak et al., 2011; Hirschmann et al., 2011), and between SMA and the STN (Lalo et al., 2008; Oswal et al., 2016). Movement-related beta responses was detected not only in the M1, but also in the

Table 3
Statistical analysis of the beta and the gamma band power.

Within group effect	Power	Post hoc comparisons
LOCATION	$F_{5,95} = 12.92$; $p < 0.001$	All comparisons: $p < 0.01$; except: $p_{M1\text{-}DLPFC}$, $p_{M1\text{-}CER}$, $p_{DLPFC\text{-}CER}$
BAND	$F_{1,19} = 64558$; $p < 0.001$	$p_{BETA\text{-}GAMMA} < 0.001$
BAND × SUBBAND	$F_{1,19} = 10048$; $p < 0.001$	All comparisons: $p < 0.01$
STIMULATION LEVEL	$F_{3,57} = 39$; $p < 0.001$	All comparisons: $p < 0.05$
BAND × STIMULATION LEVEL	$F_{3,57} = 2783$; $p < 0.001$	All comparisons: $p < 0.001$
TASK	$F_{3,57} = 250$; $p < 0.001$	All comparisons: $p < 0.001$
BAND × TASK	$F_{3,57} = 361$; $p < 0.001$	All comparisons: $p < 0.001$; except: $p_{BETA:FT\text{-}PS} = 0.08$
LOCATION × TASK	$F_{15,285} = 53$; $p < 0.001$	Resting state: $p_{M1\text{-}PMC} < 0.001$; $p_{M1\text{-}SMA} < 0.001$; $p_{M1\text{-}STN} < 0.001$. Finger tapping: $p_{M1\text{-}STN} < 0.001$. Pronation-supination: $p_{M1\text{-}SMA} < 0.001$; $p_{M1\text{-}STN} < 0.001$. Hand grasping: $p_{M1\text{-}SMA} < 0.001$; $p_{M1\text{-}STN} < 0.001$.
HEMISPHERE	$F_{1,19} = 14206$; $p < 0.001$	$p_{CONTRA\text{-}IPSI} < 0.001$
TASK × HEMISPHERE	$F_{3,57} = 253$; $p < 0.001$	$p_{CONTRA\text{-}IPSI} < 0.001$ in all tasks
LOCATION × BAND	$F_{5,95} = 323$; $p < 0.001$	Comparisons of location M1: $p < 0.001$; except: $p_{BETA:M1\text{-}DLPFC}$:0.99; $p_{BETA:M1\text{-}CER}$:0.99; $p_{GAMMA:M1\text{-}PMC}$:0.8; $p_{GAMMA:M1\text{-}DLPFC}$:0.53; $p_{GAMMA:M1\text{-}CER}$:0.59
STIMULATION LEVEL × HEMISPHERE	$F_{3,57} = 50$; $p < 0.001$	All comparisons: $p < 0.001$; except all comparisons between ipsilateral values (contralateral in the cerebellum): $p > 0.19$

Contralateral (contra): contralateral to the movement; Ipsilateral (ipsi): ipsilateral to the movement.

PMC (Pollok et al., 2009), as well as in the SMA (Pollok et al., 2009). It has been demonstrated in animals that corticosubthalamic fibers originate in the M1, PMC, and the SMA (Nambu et al., 1997; Inase et al., 1999).

The motor cortex areas may not have a primary role in the generation of beta activity (Guerra et al., 2021), which may be part of the neuroplastic responses to dopamine depletion (Hirschmann et al., 2013; Abbasi et al., 2018; Luoma et al., 2018). The hierarchical arrangement in these networks has not yet been established. STN-cortical coupling is bidirectional and dynamically changes in brain states, as was deduced in both animal (West et al., 2018) and human studies (Lalo et al., 2008; Shimamoto et al., 2013). Our results also pinpointed the complex network nature of the pathophysiology behind bradykinesia, in which M1 and the premotor cortex play a determining role.

The association of beta power on a network level with the real-time kinematic parameters was strong (standardized coefficient: 0.65–0.81). In a study by Neumann et al., the correlation coefficient was $r = 0.44$ between beta power in the STN and the Unified Parkinson's Disease Rating Scale scores in a cohort of 63 patients (Neumann et al., 2016). It was $r = 0.70$ when correlating beta power in the primary sensorimotor cortex and the Unified Parkinson's Disease Rating Scale scores across 20 patients (Pollok et al., 2012). Frontal gamma (55–65 Hz) power rise evoked by STN-DBS correlated with the Unified Parkinson's Disease Rating Scale III. Scores in 13 patients; $r = 0.765$ (Cao et al., 2017); these results also draw attention to the cortical activity, which may additionally improve the sensitivity and specificity of beta and gamma activity as oscillatory markers of bradykinesia.

Our results propose that complex cortical-subcortical models are necessary to administer the voluntary movements in PD patients during deep brain stimulation. The cortical inputs did not significantly predict the outcome variables in all four significant models that we found, only if cortical and subcortical input was combined. This led us to the assumption that the slope of activity (dynamic changes over the four stimulation conditions) in specific cortical-subcortical loops predicts the slope of the kinematic variables. Other studies also support the hypothesis. It was shown earlier that speed-accuracy adjustments of finger tapping are controlled by two distinct subloop between STN and the frontal cortex in PD patients similarly that we present in the first model (Herz et al., 2017). In all the other three models, we were able to predict the amplitude of the movement from mediator sub-cortical loop activities, which has been shown in several STN and motor cortex recordings in the beta frequency range (Androulidakis et al., 2008; Khawaldeh et al., 2021; Kondylis et al., 2016). And, force of hand-grasping related to low beta frequency in the sensorimotor cortices on scalp EEG recordings (Darch et al., 2020; Zaepffel et al., 2013).

4.2. Beta and gamma sub-bands in the motor system

Based on previous research, we opted to investigate beta (Wang et al., 2018; Oswal et al., 2016; Lofredi et al., 2019) and gamma subbands (Cao et al., 2017), given that their function is likely to be different in the basal ganglia-thalamo-cortical system. The reactivity of the low beta band to levodopa (Litvak et al., 2011) and DBS (Oswal et al., 2016) in the STN correlated with the clinical improvement, while high beta band activity was shown to be dominant in the cortico-subthalamic connectivity (Oswal et al., 2016; Litvak et al., 2011). The appearance of low frequency beta bursts in the STN worsened movement performance (Lofredi et al., 2019). In our study, symptom-predicting beta activity appeared in both low and high band in the M1-PMC-STN circuit, while the M1-SMA-STN circuit drove on the low beta frequency.

We analyzed gamma activation in the 31–100 Hz range in two subbands; as the higher range encompassed the 60–90 Hz narrow-band gamma activity, which was identified in the M1-STN interaction (Litvak et al., 2012) and may have symptom-specificity (Swann et al., 2016). High frequency gamma activity in the PMC-DLPFC-CER network was predictive for movement speed in our study, this network activity was also captured in different hand movements in healthy subjects (Tamás et al., 2018). The role of cerebellum has also been raised in the development of bradykinesia through motor feedback processing due to its connections with the basal ganglia and the sensorimotor cortex areas (Bologna et al., 2020).

In our study, movement action did not affect low and high frequency beta and gamma power compared to the resting state. Several studies measuring STN-LFP and simultaneously cortical activity in the perioperative state have reported that gamma band power increases during movements compared to resting state in the STN (Florin et al., 2013), and on the cortical level (Rowland et al., 2015). However, high, and low frequency gamma activity was lower in the resting state than during movement only in the STN in our study, similarly to an EEG and STN-LFP study, in which movement significantly enhanced gamma activity in the STN, SMA but not in the M1. Our results from chronically stimulation patients suggest that STN-DBS, similar to dopamine (Lofredi et al., 2018), increases low and high-frequency gamma activity, which facilitates but does not encode movement processes (Muthukumaraswamy, 2010) in the contralateral hemisphere. de Hemptinne et al. (2015) examined cortical gamma activity gamma during rest and a movement task before, during, and after activated STN-DBS. They show higher broadband gamma (50–200 Hz) activity during movement than in rest, not affected by the activated STN-DBS. However, they examined patients after the lead insertion and could not exclude the modifying effect of propofol, and they had not tested the stimulation site and parameters before screening. Thus, further studies are needed to explore this effect of STN-DBS. Similarly, we did not experience movement-

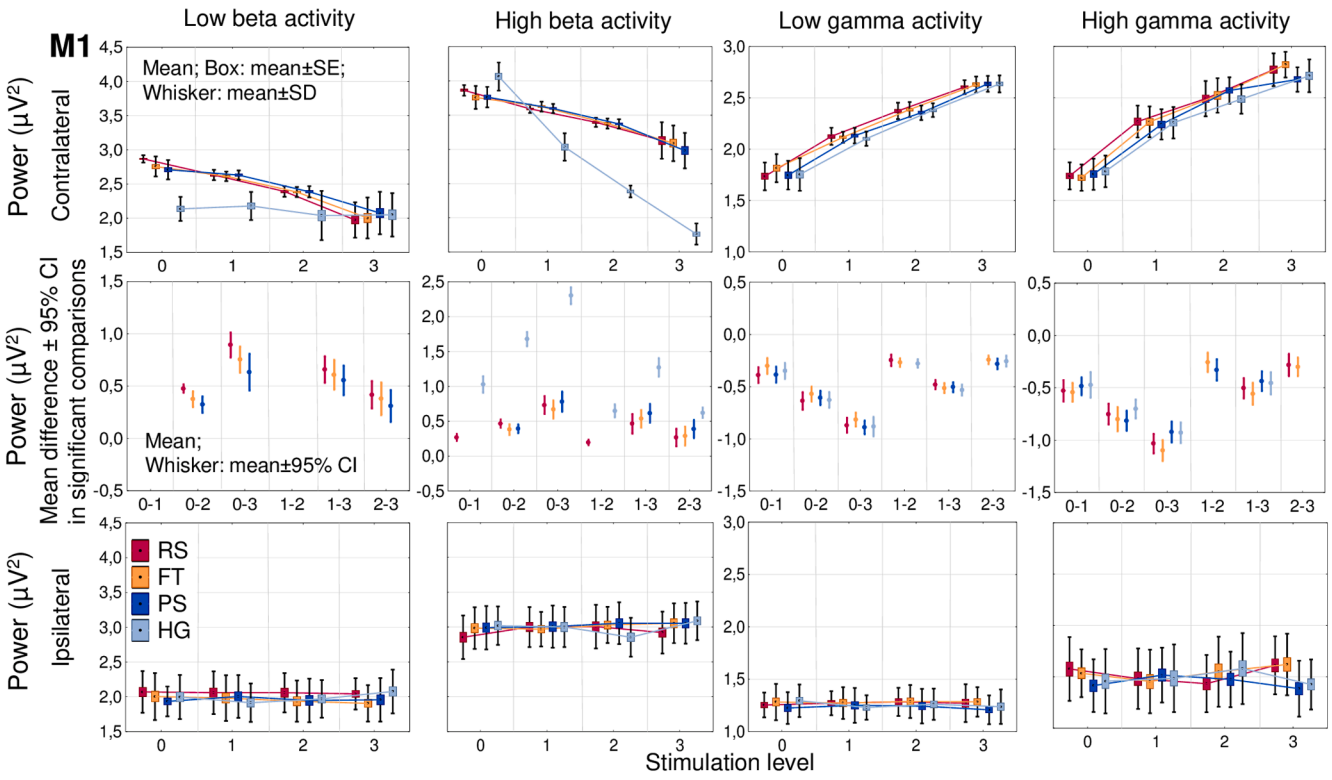

Fig. 6. Absolute beta and gamma power values in the primary motor cortex (M1) during screening Low and high frequency beta power decreased, low and high frequency gamma power increased with raising stimulation intensity contralateral but not ipsilateral to the examined hand. In the middle row, we present the mean and the 95% confidence interval of the individual power differences between stimulation conditions, contralateral to the movement, in the significant repeated measures comparisons.

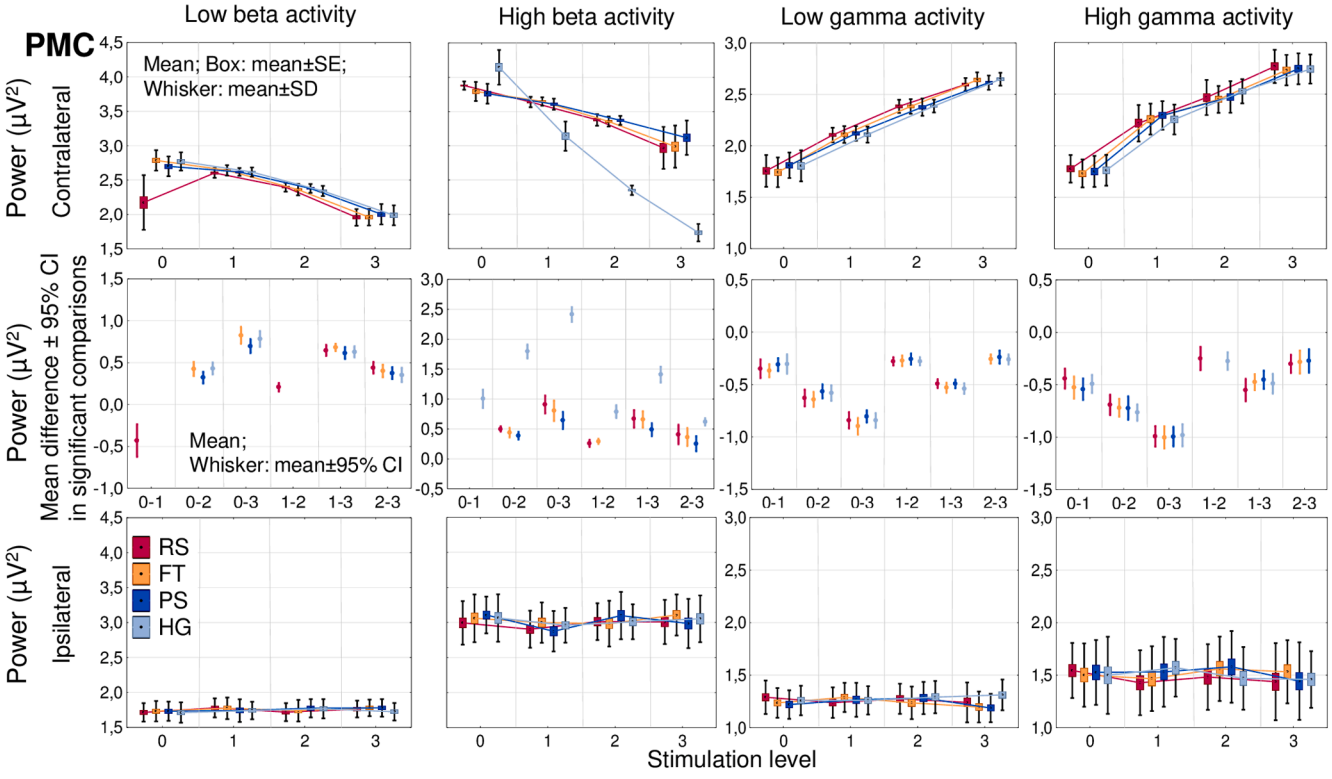

Fig. 7. Absolute beta and gamma power values in the premotor cortex (PMC) during screening Beta and gamma power changes are similar to changes in the primary motor cortex.

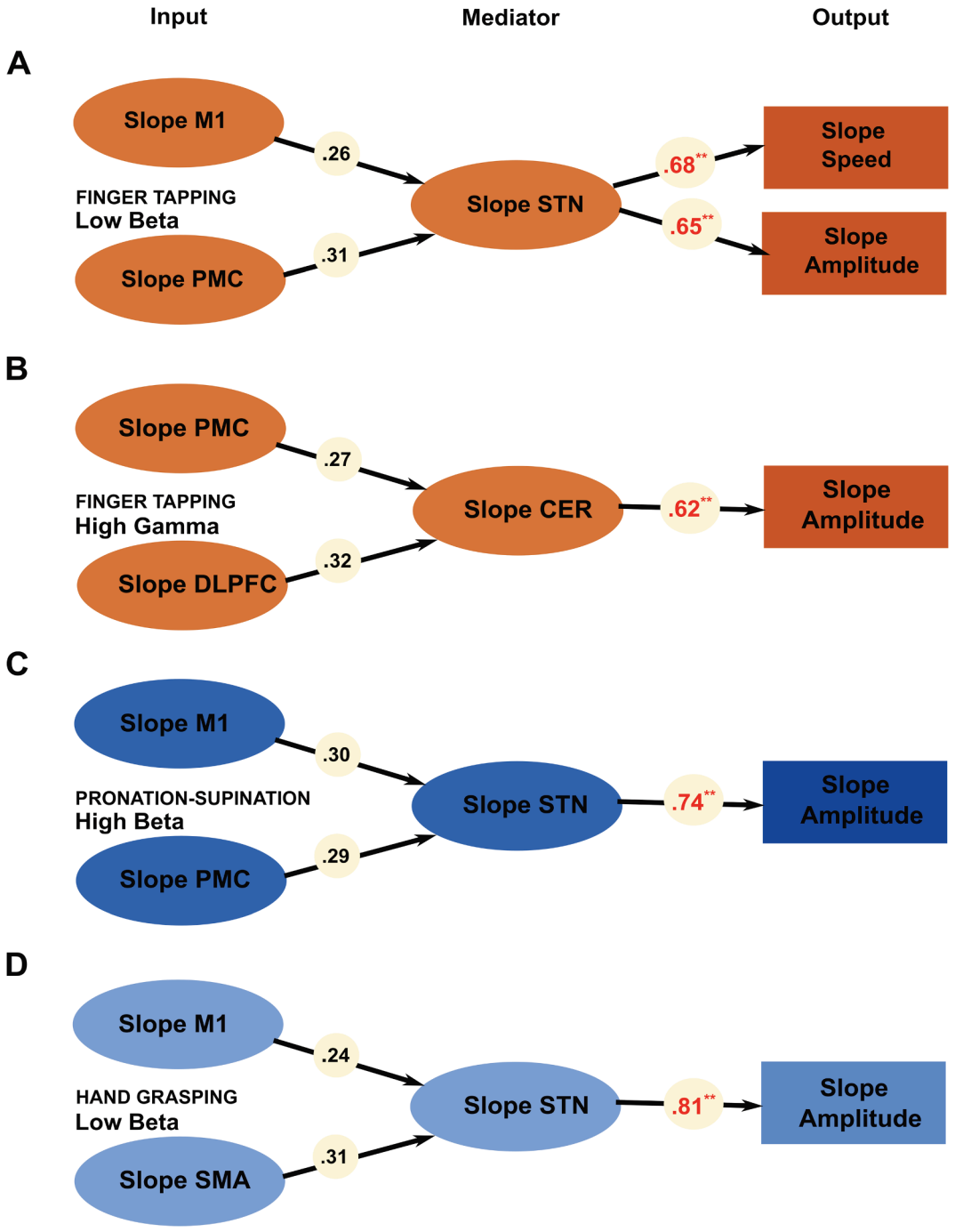

Fig. 8. Relationships between slope of changes in the Kinesia scores and the slope of changes in the power Network activities predicted the parameters of the movement in the models (A-D). Standardized coefficients significant at $p < 0.01$ are shown in red.

related beta desynchronization in different stimulation conditions even in STIM OFF in our study. Beta power decrease was measured earlier on the cortical level in Parkinson's disease (Rowland et al., 2015; Meziane et al., 2015), although it is diminished compared to the power changes in controls (Heinrichs-Graham et al., 2014). An LFP recording found movement-related beta desynchronization in the STN (Litvak et al., 2012), but another study observed an excessive beta activity not reacting to movement execution (Florin et al., 2013). Thus, impaired beta power decrease during movement may be a sign of diminished movement capacity in PD (Heinrichs-Graham et al., 2014).

4.3. Cortical effect of STN stimulation in the two hemispheres

STN-DBS decreased low and high frequency beta power in the assessed network nodes while increased gamma power in the hemisphere on the same side and the cerebellum on the other side. Previous investigations reported similar DBS effects. DBS evoked a decrease in beta power in the STN while Parkinson's disease patients performed a pronation-supination task (Kühn et al., 2008), and also in the central cortical region in a resting state (Whitmer et al., 2012) and during upper limb movement (Abbasi et al., 2018; Luoma et al., 2018). An increase in the frontal gamma (55–65 Hz) band activity during STN-DBS also correlated with remission of motor symptoms in a

magnetoencephalography study (Cao et al., 2017).

We found that STN-DBS strictly affected the hemisphere on the same side and the cerebellum on the other side while the contralateral STN was continuously stimulated, presuming its decisive action in the ipsilateral functional network. Unilateral STN-DBS was shown to attenuate beta power over the bilateral sensorimotor, secondary sensory, premotor areas, and the supplementary motor cortex, but was more pronounced on the ipsilateral side (Abbasi et al., 2018). This observation is in accordance with clinical findings that STN-DBS exerts effects on bilateral body parts but with strong contralateral preponderance (Slowinski et al., 2007). Anatomical data confirmed that the cortico-subthalamic fibers also project exclusively to the ipsilateral STN (Romanelli et al., 2005). Our results align with the observations that gamma activity occurs contralateral to the movement (Alegre et al., 2005; Crone et al., 1998). The more extensive low and high-frequency gamma activity contralateral compared to the ipsilateral side even in rest may imply that patients turned their attention to their examined hand (Wöstmann et al., 2018), and motor imagery might evoke an increase in the activity (Fischer et al., 2017; Miller et al., 2010). Higher gamma power in the hemisphere contralateral to the movement could also be a result of a more pronounced compensatory mechanism in the more affected than the less affected motor network (Rowland et al., 2015; Hemptinne et al., 2019) as we examined the more affected hand and the related motor network.

4.4. Beta and gamma power in different tasks

The three different tasks evoked different changes in subnetwork activities. Especially, the underlying activity of hand grasping differed from that of finger tapping or pronation-supination. During hand grasping, low frequency beta activity in M1, DLPFC, and the CER did not change with increasing stimulation. However, high beta activity fell significantly with higher stimulation amplitude in all locations. In the SMA, low beta and high gamma activity were continuously low during hand grasping irrespective of increasing stimulation intensity, similarly to low beta activity in the SMA. The anatomical organization can explain the difference between observation in hand grasping and finger tapping.

It was already observed that finger tapping as the most distal hand movement reacts equally to contralateral and bilateral stimulation. Hand grasping or pronation supination needs bilateral stimulation for better improvement (Tamás et al., 2016). Finger tapping is directed by exclusively ipsilateral cortico-subthalamic pathways, on which the stimulation acts antidromically (Inase et al., 1999). More proximal muscles are innervated from the bilateral motor cortex areas, mainly the PM and the SMA (Alexander et al., 1986; Montgomery et al., 2013). However, we cannot exclude that fatigue effect influenced the measurements during hand grasping, while we did not randomize the order of hand movements. Patients performed finger tapping first, then pronation supination, and finally, hand grasping. However, our results confirm that during finger tapping movement, beta activity decreases, and gamma increases in all locations.

4.5. STN-DBS improves the speed and amplitude of the movement

The Kinesia scores we computed from the speed, amplitude and rhythm have the advantage over the more often used clinical scales that movement parameters are equally weighted as opposed to the observation that speed is less noticed by clinical raters than amplitude and rhythm (Heldman et al., 2011). These parameters also have different reactivity to levodopa and DBS therapy. Speed improves predominantly after levodopa treatment (Espay et al., 2011). Speed and amplitude improved the most with increasing contralateral stimulation intensity in our study; the rhythm was the least affected. Decrement of speed and amplitude was not influenced by stimulation similarly to our previous results (Tamás et al., 2016); it also did not improve after a levodopa challenge test (Espay et al., 2011). The accuracy of our results is enhanced by using Kinesia scores; this method can capture even subtle changes in bradykinesia in response to small adjustment of DBS (Pulliam et al., 2015).

4.6. Methodological considerations and limitations

DICS is a powerful technique of electrical source imaging that investigates neuronal interactions by imaging power estimates of oscillatory brain activity (Gross et al., 2001). DICS can characterize networks associated with different types of tremor and voluntary motor control (Gross et al., 2001; Gross et al., 2002; Timmermann et al., 2003). It is noteworthy that not only cortical sources but also sources in deep structures such as in the diencephalon (e.g., the thalamus) and the cerebellum were detected using DICS (Gross et al., 2001; Gross et al., 2002; Timmermann et al., 2003; Schnitzler et al., 2009; Südmeyer et al., 2006). In this study, we reveal brain sources in subcortical regions such as the STN and cerebellum. It has been a matter of debate for many years whether it is possible to find subcortical sources based on recordings on the scalp. In previous MEG (Südmeyer et al., 2006) and EEG (Muthuraman et al., 2012) studies on patients, as well as in an EEG study on healthy subjects (Tamás et al., 2018); subcortical sources have been detected by applying DICS to oscillatory signals. However, the interpretation of the results on the sub-cortical sources needs to be assessed carefully.

It has been generally assumed that only cortical sources of at least 6.25 cm^2 might be registered using the scalp EEG (Hara et al., 1999). Intracranial recordings suggest that spikes arising from deeper structures such as the mesial temporal lobe might only be detected by the scalp EEG when averaged (Merlet et al., 1998). However, DICS differs from the techniques in the mentioned studies in several ways. Dipolar and distributed source modelling aims to localize sources of electric currents in the brain that give rise to potential fields at the scalp. However, the DICS analysis does not try to explain the signal recorded on the scalp EEG by single sources but looks for sources that are coherent to a given reference signal. Since only a specific frequency range of interest is analyzed, this method can detect even small oscillatory activity in this frequency range. There are different types of support showing that DICS is also sensitive to deep sources. It is known that over-regularization may lead to “ghost sources” in the middle of the brain. However, in all our analyses, we used the same moderate value for regularization, which has been shown to yield adequate results (Kujala et al., 2008). When DICS was applied to simulated distributed large sources restricted to the cortex, no artificially located midline subcortical sources were detected. This result underlines the fact that the coherence is restricted to the sources revealed by DICS. In addition, even sources of weak physiological oscillatory activity have been detected in the thalamus using a similar source analysis approach on MEG data (Cantero et al., 2009). The general dogma that surface recordings cannot identify deep subcortical sources has been questioned (Kimura et al., 2008).

Furthermore, our previous work identified STN and cerebellum activity during finger tapping using the same method and 64-channel EEG system (Muthuraman et al., 2014). Based on these results, we used the finger tapping EMG signal as the reference signal in the present study to identify stable cortical and sub-cortical sources.

Another question may arise, how the results are affected by the artifact of the DBS stimulation. If the endogenous beta and gamma frequency were narrowband and uniformly a subharmonic of the stimulation frequency, the clusters would be specifically at frequencies of 65 Hz (effective stimulation at 130 Hz). However, our results showed that the power in the plots was not so precisely tuned (Supplementary Fig. 2; especially in SMA, STN, and Cerebellum). This might relate to inter-individual differences in the peak frequencies of endogenous gamma activity, whereby an endogenous oscillation that is not at a precise subharmonic of the stimulation frequency may still be close enough to this subharmonic frequency be subject to resonance, and its amplitude

would increase during stimulation. Its probability depends on the frequency difference between the endogenous gamma and the stimulation harmonic activity and upon the degree of damping in the endogenous gamma oscillation according to the severity of the symptoms. The higher the damping, the less will be the shifting frequency of the endogenous gamma towards the subharmonic of stimulation, the smaller the increase in amplitude due to the driving frequency.

The damping of the endogenous oscillation is a key factor in dictating the behavior of the oscillation when forced by a driving frequency, in this case, the DBS and its' subharmonic. Hence it may be important to note that stimulation was performed in the OFF-medication state in our paradigm when endogenous gamma is not so highly tuned and is attenuated, consistent with damping of the oscillation. In addition, the power differences are not specific for each task and resting state over the frequency bands, so we cannot rule out that pure artifact of the DBS stimulation influenced the results.

5. Conclusions

Our results confirmed that changes in the beta and gamma activity of different subnetworks predict bradykinesia, in which the M1 and PMC are common nodes. Adaptive deep brain stimulation is a new direction in the development of DBS. Our results denote that both cortical and subcortical sensor placements would be beneficial in capturing bradykinesia reliably and that multiple frequency sub-bands should be parallel detected, as they are specific for different subnetworks.

CRediT authorship contribution statement

Muthuraman Muthuraman: Conceptualization, Methodology, Software, Validation, Formal analysis, Data curation, Writing – original draft, Visualization, Supervision, Funding acquisition. **Marcell Palotai:** Investigation, Writing – review & editing, Visualization. **Borbála Jávor-Duray:** Methodology, Validation, Formal analysis, Investigation, Data curation, Writing – review & editing. **Andrea Kelemen:** Investigation, Writing – review & editing. **Nabin Koirala:** Methodology, Formal analysis, Data curation, Writing – review & editing, Visualization. **László Halász:** Data curation, Writing – review & editing. **Loránd Erőss:** Data curation, Writing – review & editing. **Gábor Fekete:** Data curation, Writing – review & editing. **László Bognár:** Writing – review & editing. **Günther Deuschl:** Conceptualization, Writing – review & editing, Funding acquisition. **Gertrúd Tamás:** Conceptualization, Methodology, Validation, Formal analysis, Investigation, Resources, Data curation, Writing – original draft, Visualization, Supervision, Project administration, Funding acquisition.

Declaration of Competing Interest

The authors declare that they have no known competing financial interests or personal relationships that could have appeared to influence the work reported in this paper.

Acknowledgement

We would like to thank our patients for their committed participation in the study. Medtronic plc. provided partial fund for the study (NM-2949). The funding source neither influenced the study design, collection, analysis, the interpretation of data, nor any decisions to submit the paper for publication.

Appendix A. Supplementary data

Supplementary data to this article can be found online at https://doi.org/10.1016/j.nicl.2021.102857.

References

de Hemptinne, C., Swann, N.C., Ostrem, J.L., Ryapolova-Webb, E.S., San Luciano, M., Galifianakis, N.B., Starr, P.A., 2015. Therapeutic deep brain stimulation reduces cortical phase-amplitude coupling in Parkinson's disease. Nat. Neurosci. 18 (5), 779–786.

Neumann, W.-J., Degen, K., Schneider, G.-H., Brücke, C., Huebl, J., Brown, P., Kühn, A. A., 2016. Subthalamic synchronized oscillatory activity correlates with motor impairment in patients with Parkinson's disease. Mov. Disord. 31 (11), 1748–1751.

Mallet, N., Pogosyan, A., Sharott, A., Csicsvari, J., Bolam, J.P., Brown, P., Magill, P.J., 2008. Disrupted dopamine transmission and the emergence of exaggerated beta oscillations in subthalamic nucleus and cerebral cortex. J. Neurosci. 28 (18), 4795–4806.

West, T.O., Berthouze, L., Halliday, D.M., Litvak, V., Sharott, A., Magill, P.J., Farmer, S. F., 2018. Propagation of beta/gamma rhythms in the cortico-basal ganglia circuits of the parkinsonian rat. J. Neurophysiol. 119 (5), 1608–1628.

Kühn, A.A., Kempf, F., Brücke, C., et al., 2008. High-frequency stimulation of the subthalamic nucleus suppresses oscillatory beta activity in patients with Parkinson's disease in parallel with improvement in motor performance. J Neurosci. 28 (24), 6165–6173.

Hirschmann, J., Özkurt, T.E., Butz, M., Homburger, M., Elben, S., Hartmann, C.J., Vesper, J., Wojtecki, L., Schnitzler, A., 2013. Differential modulation of STN-cortical and cortico-muscular coherence by movement and levodopa in Parkinson's disease. Neuroimage. 68, 203–213.

Lalo, E., Thobois, S., Sharott, A., Polo, G., Mertens, P., Pogosyan, A., Brown, P., 2008. Patterns of bidirectional communication between cortex and basal ganglia during movement in patients with Parkinson disease. J. Neurosci. 28 (12), 3008–3016.

Pollok, B., Kamp, D., Butz, M., Wojtecki, L., Timmermann, L., Südmeyer, M., Krause, V., Schnitzler, A., 2013. Increased SMA-M1 coherence in Parkinson's disease - Pathophysiology or compensation? Exp. Neurol. 247, 178–181.

Wang, D.D., de Hemptinne, C., Miocinovic, S., Ostrem, J.L., Galifianakis, N.B., San Luciano, M., Starr, P.A., 2018. Pallidal deep-brain stimulation disrupts pallidal beta oscillations and coherence with primary motor cortex in parkinson's disease. J. Neurosci. 38 (19), 4556–4568.

Steiner, L.A., Neumann, W.-J., Staub-Bartelt, F., Herz, D.M., Tan, H., Pogosyan, A., Kuhn, A.A., Brown, P., 2017. Subthalamic beta dynamics mirror Parkinsonian bradykinesia months after neurostimulator implantation. Mov. Disord. 32 (8), 1183–1190.

D. Williams A. Kühn A. Kupsch M. Tijssen G. van Bruggen H. Speelman G. Hotton C. Loukas P. Brown The relationship between oscillatory activity and motor reaction time in the parkinsonian subthalamic nucleus 21 1 2005 249 258.

Kühn, A.A., Tsui, A., Aziz, T., Ray, N., Brücke, C., Kupsch, A., Schneider, G.-H., Brown, P., 2009. Pathological synchronisation in the subthalamic nucleus of patients with Parkinson's disease relates to both bradykinesia and rigidity. Exp. Neurol. 215 (2), 380–387.

Ray, N.J., Jenkinson, N., Wang, S., Holland, P., Brittain, J.S., Joint, C., Stein, J.F., Aziz, T., 2008. Local field potential beta activity in the subthalamic nucleus of patients with Parkinson's disease is associated with improvements in bradykinesia after dopamine and deep brain stimulation. Exp. Neurol. 213 (1), 108–113.

Oswal, A., Beudel, M., Zrinzo, L., Limousin, P., Hariz, M., Foltynie, T., Litvak, V., Brown, P., 2016. Deep brain stimulation modulates synchrony within spatially and spectrally distinct resting state networks in Parkinson's disease. Brain 139 (5), 1482–1496.

Whitmer, D., de Solages, C., Hill, B., Yu, H., Henderson, J.M., Bronte-Stewart, H., 2012. High frequency deep brain stimulation attenuates subthalamic and cortical rhythms in Parkinson's disease. Front. Hum. Neurosci. 6, 155.

Abbasi, O., Hirschmann, J., Storzer, L., Özkurt, T.E., Elben, S., Vesper, J., Wojtecki, L., Schmitz, G., Schnitzler, A., Butz, M., 2018. Unilateral deep brain stimulation suppresses alpha and beta oscillations in sensorimotor cortices. Neuroimage 174, 201–207.

Luoma, J., Pekkonen, E., Airaksinen, K., Helle, L., Nurminen, J., Taulu, S., Mäkelä, J.P., 2018. Spontaneous sensorimotor cortical activity is suppressed by deep brain stimulation in patients with advanced Parkinson's disease. Neurosci. Lett. 683, 48–53.

Pollok, B., Krause, V., Martsch, W., Wach, C., Schnitzler, A., Südmeyer, M., 2012. Motor-cortical oscillations in early stages of Parkinson's disease. J. Physiol. 590 (13), 3203–3212.

Tamás, G., Chirumamilla, V.C., Anwar, A.R., Raethjen, J., Deuschl, G., Groppa, S., Muthuraman, M., 2018. Primary sensorimotor cortex drives the common cortical network for gamma synchronization in voluntary hand movements. Front. Hum. Neurosci. 12 https://doi.org/10.3389/fnhum.2018.00130.

Litvak, V., Eusebio, A., Jha, A., Oostenveld, R., Barnes, G., Foltynie, T., Limousin, P., Zrinzo, L., Hariz, M.I., Friston, K., Brown, P., 2012. Movement-related changes in local and long-range synchronization in Parkinson's disease revealed by simultaneous magnetoencephalography and intracranial recordings. J. Neurosci. 32 (31), 10541–10553.

Lofredi R, Neumann WJ, Bock A, et al. Dopamine-dependent scaling of subthalamic gamma bursts with movement velocity in patients with Parkinson's disease. Elife. 2018 Feb 1;7.

Swann, N.C., de Hemptinne, C., Miocinovic, S., Qasim, S., Wang, S.S., Ziman, N., Ostrem, J.L., San Luciano, M., Galifianakis, N.B., Starr, P.A., 2016. Gamma oscillations in the hyperkinetic state detected with chronic human brain recordings in parkinson's disease. J. Neurosci. 36 (24), 6445–6458.

Shimamoto, S.A., Ryapolova-Webb, E.S., Ostrem, J.L., Galifianakis, N.B., Miller, K.J., Starr, P.A., 2013. Subthalamic nucleus neurons are synchronized to primary motor cortex local field potentials in Parkinson's disease. J. Neurosci. 33 (17), 7220–7233.

Rosa, M., Marceglia, S., Servello, D., Foffani, G., Rossi, L., Sassi, M., Mrakic-Sposta, S., Zangaglia, R., Pacchetti, C., Porta, M., Priori, A., 2010. Time dependent subthalamic local field potential changes after DBS surgery in Parkinson's disease. Exp. Neurol. 222 (2), 184–190.
Bologna, M., Paparella, G., Fasano, A., Hallett, M., Berardelli, A., 2020. Evolving concepts on bradykinesia. Brain. 143 (3), 727–750.
Espay, A.J., Giuffrida, J.P., Chen, R., Payne, M., Mazzella, F., Dunn, E., Vaughan, J.E., Duker, A.P., Sahay, A., Kim, S.J., Revilla, F.J., Heldman, D.A., 2011. Differential response of speed, amplitude, and rhythm to dopaminergic medications in Parkinson's disease. Mov. Disord. 26 (14), 2504–2508.
Heldman, D.A., Giuffrida, J.P., Chen, R., Payne, M., Mazzella, F., Duker, A.P., Sahay, A., Kim, S.J., Revilla, F.J., Espay, A.J., 2011. The modified bradykinesia rating scale for Parkinson's disease: reliability and comparison with kinematic measures. Mov. Disord. 26 (10), 1859–1863.
Pulliam, C.L., Heldman, D.A., Orcutt, T.H., Mera, T.O., Giuffrida, J.P., Vitek, J.L., 2015. Motion sensor strategies for automated optimization of deep brain stimulation in Parkinson's disease. Parkinsonism Relat Disord. 21 (4), 378–382.
Andrade-Souza YM, Schwalb JM, Hamani C, et al. Comparison of three methods of targeting the subthalamic nucleus for chronic stimulation in Parkinson's disease. Neurosurgery. 2005 Apr;56(2 Suppl):360-8; discussion -8.
Tamás, G., Kelemen, A., Radics, P., Valálik, I., Heldman, D., Klivényi, P., Vécsei, L., Hidasi, E., Halász, L., Kis, D., Barsi, P., Golopencza, P., Erőss, L., 2016. Effect of subthalamic stimulation on distal and proximal upper limb movements in Parkinson's disease. Brain Res. 1648, 438–444.
Horn, A., Kühn, A.A., 2015. Lead-DBS: a toolbox for deep brain stimulation electrode localizations and visualizations. Neuroimage. 15 (107), 127–135.
Horn, A., Li, N., Dembek, T.A., Kappel, A., Boulay, C., Ewert, S., Tietze, A., Husch, A., Perera, T., Neumann, W.-J., Reisert, M., Si, H., Oostenveld, R., Rorden, C., Yeh, F.-C., Fang, Q., Herrington, T.M., Vorwerk, J., Kühn, A.A., 2019. Lead-DBS v2: towards a comprehensive pipeline for deep brain stimulation imaging. Neuroimage. 184, 293–316.
Horn, A., Reich, M., Vorwerk, J., Li, N., Wenzel, G., Fang, Q., Schmitz-Hübsch, T., Nickl, R., Kupsch, A., Volkmann, J., Kühn, A.A., Fox, M.D., 2017. Connectivity predicts deep brain stimulation outcome in Parkinson disease. Ann. Neurol. 82 (1), 67–78.
Åström, M., Zrinzo, L.U., Tisch, S., Tripoliti, E., Hariz, M.I., Wårdell, K., 2009. Method for patient-specific finite element modeling and simulation of deep brain stimulation. Med. Biol. Eng. Compu. 47 (1), 21–28.
Oostenveld, R., Fries, P., Maris, E., Schoffelen, J.-M., 2011. FieldTrip: open source software for advanced analysis of MEG, EEG, and invasive electrophysiological data. Comput. Intell. Neurosci. 2011, 1–9.
Mitra, P.P., Pesaran, B., 1999. Analysis of dynamic brain imaging data. Biophys. J. 76 (2), 691–708.
Muthuraman, M., Heute, U., Deuschl, G., Raethjen, J., 2010. The central oscillatory network of essential tremor. Conf. Proc. IEEE Eng. Med. Biol. Soc. 2010, 154–157.
Slepian, D., Pollak, H.O., 1961. Prolate spheroidal wave functions, fourier analysis and uncertainty — I. Bell Syst. Tech. J. 40 (1), 43–63.
Muthuraman, M., Galka, A., Deuschl, G., Heute, U., Raethjen, J., 2010. Dynamical correlation of non-stationary signals in time domain—A comparative study. Biomed. Signal Process. Control 5 (3), 205–213.
Wolters, C.H., Anwander, A., Berti, G., Hartmann, U., 2007. Geometry-adapted hexahedral meshes improve accuracy of finite-element-method-based EEG source analysis. IEEE Trans. Biomed. Eng. 54 (8), 1446–1453.
Muthuraman M, Raethjen J, Koirala N, et al. Cerebello-cortical network fingerprints differ between essential, Parkinson's and mimicked tremors. Brain. 2018 Jun 1;141 (6):1770-81.
Van Veen, B.D., van Drongelen, W., Yuchtman, M., Suzuki, A., 1997. Localization of brain electrical activity via linearly constrained minimum variance spatial filtering. IEEE Trans. Biomed. Eng. 44 (9), 867–880.
Muthuraman, M., Heute, U., Arning, K., Anwar, A.R., Elble, R., Deuschl, G., Raethjen, J., 2012. Oscillating central motor networks in pathological tremors and voluntary movements. What makes the difference? Neuroimage. 60 (2), 1331–1339.
Anwar, A.R., Muthalib, M., Perrey, S., Galka, A., Granert, O., Wolff, S., Heute, U., Deuschl, G., Raethjen, J., Muthuraman, M., 2016. Effective connectivity of cortical sensorimotor networks during finger movement tasks: a simultaneous fNIRS, fMRI. EEG Study. Brain Topogr. 29 (5), 645–660.
Muthuraman, M., Hellriegel, H., Hoogenboom, N., Anwar, A.R., Mideksa, K.G., Krause, H., Schnitzler, A., Deuschl, G., Raethjen, J., Di Russo, F., 2014. Beamformer source analysis and connectivity on concurrent EEG and MEG data during voluntary movements. PLoS ONE 9 (3), e91441.
Pollok, B., Butz, M., Gross, J., Schnitzler, A., 2007. Intercerebellar coupling contributes to bimanual coordination. J. Cogn. Neurosci. 19 (4), 704–719.
Pollok, B., Krause, V., Butz, M., Schnitzler, A., 2009. Modality specific functional interaction in sensorimotor synchronization. Hum. Brain Mapp. 30 (6), 1783–1790.
Amjad, A.M., Halliday, D.M., Rosenberg, J.R., Conway, B.A., 1997. An extended difference of coherence test for comparing and combining several independent coherence estimates: theory and application to the study of motor units and physiological tremor. J. Neurosci. Methods 73 (1), 69–79.
Rosenberg, J.R., Amjad, A.M., Breeze, P., Brillinger, D.R., Halliday, D.M., 1989. The Fourier approach to the identification of functional coupling between neuronal spike trains. Prog. Biophys. Mol. Biol. 53 (1), 1–31.
Muthuraman M, Bange M, Koirala N, et al. Cross-frequency coupling between gamma oscillations and deep brain stimulation in cortico-subcortical networks in Parkinson's disease patients Brain. 2020;In press.
Lofredi, R., Tan, H., Neumann, W.-J., Yeh, C.-H., Schneider, G.-H., Kühn, A.A., Brown, P., 2019. Beta bursts during continuous movements accompany the velocity decrement in Parkinson's disease patients. Neurobiol. Dis. 127, 462–471.
Cao, C.Y., Zeng, K., Li, D.Y., Zhan, S.K., Li, X.L., Sun, B.M., 2017. Modulations on cortical oscillations by subthalamic deep brain stimulation in patients with Parkinson disease: a MEG study. Neurosci. Lett. 1 (636), 95–100.
Smith, C.E., Cribbie, R.A., 2013. Multiplicity control in structural equation modeling: incorporating parameter dependencies. Struct. Equat. Model. Multidiscipl. J. 20 (1), 79–85.
Litvak V, Jha A, Eusebio A, et al. Resting oscillatory cortico-subthalamic connectivity in patients with Parkinson's disease. Brain. 2011 Feb;134(Pt 2):359-74.
Hirschmann, J., Özkurt, T.E., Butz, M., Homburger, M., Elben, S., Hartmann, C.J., Vesper, J., Wojtecki, L., Schnitzler, A., 2011. Distinct oscillatory STN-cortical loops revealed by simultaneous MEG and local field potential recordings in patients with Parkinson's disease. Neuroimage. 55 (3), 1159–1168.
Nambu, A., Tokuno, H., Inase, M., Takada, M., 1997. Corticosubthalamic input zones from forelimb representations of the dorsal and ventral divisions of the premotor cortex in the macaque monkey: comparison with the input zones from the primary motor cortex and the supplementary motor area. Neurosci. Lett. 239 (1), 13–16.
Inase, M., Tokuno, H., Nambu, A., Akazawa, T., Takada, M., 1999. Corticostriatal and corticosubthalamic input zones from the presupplementary motor area in the macaque monkey: comparison with the input zones from the supplementary motor area. Brain Res. 833 (2), 191–201.
Guerra A, Colella D, Giangrosso M, et al. Driving motor cortex oscillations modulates bradykinesia in Parkinson's disease. Brain. 2021 Jul 10.
Herz DM, Tan H, Brittain JS, et al. Distinct mechanisms mediate speed-accuracy adjustments in cortico-subthalamic networks. Elife. 2017 Jan 31;6.
Androulidakis, A.G., Brücke, C., Kempf, F., Kupsch, A., Aziz, T., Ashkan, K., Kühn, A.A., Brown, P., 2008. Amplitude modulation of oscillatory activity in the subthalamic nucleus during movement. Eur. J. Neurosci. 27 (5), 1277–1284.
Khawaldeh S, Tinkhauser G, Torrecillos F, et al. Balance between competing spectral states in subthalamic nucleus is linked to motor impairment in Parkinson's disease. Brain. 2021 Jul 15.
Kondylis, E.D., Randazzo, M.J., Alhourani, A., Lipski, W.J., Wozny, T.A., Pandya, Y., Ghuman, A.S., Turner, R.S., Crammond, D.J., Richardson, R.M., 2016. Movement-related dynamics of cortical oscillations in Parkinson's disease and essential tremor. Brain 139 (8), 2211–2223.
Darch, H.T., Cerminara, N.L., Gilchrist, I.D., Apps, R., 2020. Pre-movement changes in sensorimotor beta oscillations predict motor adaptation drive. Sci. Rep. 10 (1), 17946.
Zaepffel, M., Trachel, R., Kilavik, B.E., Brochier, T., Di Russo, F., 2013. Modulations of EEG beta power during planning and execution of grasping movements. PLoS ONE 8 (3), e60060.
Florin, E., Erasmi, R., Reck, C., Maarouf, M., Schnitzler, A., Fink, G.R., Timmermann, L., 2013. Does increased gamma activity in patients suffering from Parkinson's disease counteract the movement inhibiting beta activity? Neuroscience 237, 42–50.
Rowland, N.C., De Hemptinne, C., Swann, N.C., Qasim, S., Miocinovic, S., Ostrem, J.L., Knight, R.T., Starr, P.A., 2015. Task-related activity in sensorimotor cortex in Parkinson's disease and essential tremor: changes in beta and gamma bands. Front. Hum. Neurosci. 9 https://doi.org/10.3389/fnhum.2015.00512.
Muthukumaraswamy, S.D., 2010. Functional properties of human primary motor cortex gamma oscillations. J. Neurophysiol. 104 (5), 2873–2885.
Meziane, H.B., Moisello, C., Perfetti, B., Kvint, S., Isaias, I.U., Quartarone, A., Di Rocco, A., Ghilardi, M.F., Di Russo, F., 2015. Movement preparation and bilateral modulation of beta activity in aging and Parkinson's disease. PLoS ONE 10 (1), e0114817.
Heinrichs-Graham E, Wilson TW, Santamaria PM, et al. Neuromagnetic evidence of abnormal movement-related beta desynchronization in Parkinson's disease. Cereb Cortex. 2014 Oct;24(10):2669-78.
Slowinski, J.L., Putzke, J.D., Uitti, R.J., Lucas, J.A., Turk, M.F., Kall, B.A., Wharen, R.E., 2007. Unilateral deep brain stimulation of the subthalamic nucleus for Parkinson disease. J. Neurosurg. 106 (4), 626–632.
Romanelli, P., Esposito, V., Schaal, D.W., Heit, G., 2005. Somatotopy in the basal ganglia: experimental and clinical evidence for segregated sensorimotor channels. Brain Res. Brain Res. Rev. 48 (1), 112–128.
Alegre M, Alonso-Frech F, Rodriguez-Oroz MC, et al. Movement-related changes in oscillatory activity in the human subthalamic nucleus: ipsilateral vs. contralateral movements. Eur J Neurosci. 2005 Nov;22(9):2315-24.
Crone, N.E., Miglioretti, D.L., Gordon, B., Lesser, R.P., 1998. Functional mapping of human sensorimotor cortex with electrocorticographic spectral analysis. II. Event-related synchronization in the gamma band. Brain 121 (Pt 12), 2301–2315.
Wöstmann, M., Vosskuhl, J., Obleser, J., Herrmann, C.S., 2018. Opposite effects of lateralised transcranial alpha versus gamma stimulation on auditory spatial attention. Brain Stimul. 11 (4), 752–758.
Fischer P, Pogosyan A, Herz DM, et al. Subthalamic nucleus gamma activity increases not only during movement but also during movement inhibition. Elife. 2017 Jul 25;6.
Miller, K.J., Schalk, G., Fetz, E.E., den Nijs, M., Ojemann, J.G., Rao, R.P.N., 2010. Cortical activity during motor execution, motor imagery, and imagery-based online feedback. Proc. Natl. Acad. Sci. U.S.A. 107 (9), 4430–4435.
Hemptinne, C., Wang, D.D., Miocinovic, S., Chen, W., Ostrem, J.L., Starr, P.A., 2019. Pallidal thermolesion unleashes gamma oscillations in the motor cortex in Parkinson's disease. Mov. Disord. 34 (6), 903–911.
Alexander, G.E., DeLong, M.R., Strick, P.L., 1986. Parallel organization of functionally segregated circuits linking basal ganglia and cortex. Annu. Rev. Neurosci. 9 (1), 357–381.

Montgomery, L.R., Herbert, W.J., Buford, J.A., 2013. Recruitment of ipsilateral and contralateral upper limb muscles following stimulation of the cortical motor areas in the monkey. Exp. Brain Res. 230 (2), 153–164.
Gross, J., Kujala, J., Hamalainen, M., Timmermann, L., Schnitzler, A., Salmelin, R., 2001. Dynamic imaging of coherent sources: studying neural interactions in the human brain. Proc. Natl. Acad. Sci. U.S.A. 98 (2), 694–699.
Gross, J., Timmermann, L., Kujala, J., Dirks, M., Schmitz, F., Salmelin, R., Schnitzler, A., 2002. The neural basis of intermittent motor control in humans. Proc. Natl. Acad. Sci. U.S.A. 99 (4), 2299–2302.
Timmermann, L., Gross, J., Dirks, M., Volkmann, J., Freund, H.-J., Schnitzler, A., 2003. The cerebral oscillatory network of parkinsonian resting tremor. Brain 126 (1), 199–212.
Schnitzler, A., Münks, C., Butz, M., Timmermann, L., Gross, J., 2009. Synchronized brain network associated with essential tremor as revealed by magnetoencephalography. Mov. Disord. 24 (11), 1629–1635.
Südmeyer, M., Pollok, B., Hefter, H., Gross, J., Butz, M., Wojtecki, L., Timmermann, L., Schnitzler, A., 2006. Synchronized brain network underlying postural tremor in Wilson's disease. Mov. Disord. 21 (11), 1935–1940.
Hara, J., Musha, T., Shankle, W.R., 1999. Approximating dipoles from human EEG activity: the effect of dipole source configuration on dipolarity using single dipole models. IEEE Trans. Biomed. Eng. 46 (2), 125–129.
Merlet, I., Garcia-Larrea, L., Ryvlin, P., Isnard, J., Sindou, M., Mauguière, F., 1998. Topographical reliability of mesio-temporal sources of interictal spikes in temporal lobe epilepsy. Electroencephalogr. Clin. Neurophysiol. 107 (3), 206–212.
Kujala, J., Gross, J., Salmelin, R., 2008. Localization of correlated network activity at the cortical level with MEG. Neuroimage 39 (4), 1706–1720.
Cantero, J.L., Atienza, M., Cruz-Vadell, A., Suarez-Gonzalez, A., Gil-Neciga, E., 2009. Increased synchronization and decreased neural complexity underlie thalamocortical oscillatory dynamics in mild cognitive impairment. Neuroimage 46 (4), 938–948.
Kimura, T., Ozaki, I., Hashimoto, I., 2008. Impulse propagation along thalamocortical fibers can be detected magnetically outside the human brain. J. Neurosci. 28 (47), 12535–12538.